Geoid
Journal of Geodesy and Geomatics

Geoid Vol. 19, No. 3, 2024, 468-484

P-ISSN: 1858-2281; E-ISSN: 2442-3998

Pipeline Modeling using UAV LiDAR Technology

Iwan Q Himawan[1], Listiyo Fitri[2], Nurrohmat Widjajanti[*3], and Iqbal Hanun Azizi[3]
[1] Master Study Program in Geomatic Engineering, Department of Geodetic Engineering, Faculty of Engineering, UGM, Yogyakarta, Indonesia
[2] PT Terra Data Persada, Jakarta, Indonesia
[3] Department of Geodetic Engineering, Faculty of Engineering, UGM, Yogyakarta, Indonesia
*Corresponding author: nwidjajanti@ugm.ac.id

Received: 02122024; Revised: 11122024; Accepted: 11122024; Published: 12122024

Abstrak: Pipelines play an important role in operations in energy supply companies, whether geothermal, gas, or petroleum. Pipeline damage, such as corrosion, dents, and leaks caused by natural or human factors, must be detected. Problems with pipeline assets will indirectly impact high production prices. Pipeline asset mapping must be carried out precisely, quickly, and quietly, considering that the existence of pipelines often causes social unrest. This research analyzed the capabilities of UAV LiDAR for mapping pipelines and support in a three km-long pipeline area. The study concluded that UAV LiDAR can map the position of the pipeline, its position to the ground, the position of the support, and the height of the support on a pipeline network with a diameter of 1 m. This capability applies not only to segments in open areas but also to those covered by vegetation. When orthophoto cannot display the pipeline's existence, the LiDAR point cloud can identify it. This main pipeline, which has a 1 m diameter, 3-D mesh, and 3-D models, can also be formed well. The accuracy of the resulting map is 11.5 cm at a confidence level of 90%. The length of time required from preparation to the presentation of the pipeline longitudinal profile map is eight calendar days with ten manpower.

Keywords : UAV LiDAR; Pipeline Mapping; 3-D Model; Point Cloud

How to cite: Himawan, I. Q., Fitri, L., Widjajanti, N., and Azizi, I. H. (2024). Pipeline Modeling using UAV LiDAR Technology. *Geoid, 19*(3), 468 - 484.

Introduction

Pipelines play an important role in operations in energy supply companies, whether geothermal, gas, or petroleum. Pipeline damage, such as corrosion, dents, and leaks caused by natural or human factors, must be detected. Problems with pipeline assets will indirectly impact high production prices. Pipeline asset mapping should be carried out precisely, quickly, and quietly, considering that the existence of pipelines often causes social unrest.

The technology often used for mapping pipeline assets is terrestrial surveys with total stations and GNSS-RTK. However, these two technologies require measurements to come directly to the object and involve many personnel. The potential for friction with the community is vital. Another terrestrial method for piping measurements is Terrestrial Laser Scanning (TLS). TLS can produce millions of 3-D coordinate point clouds in a single sweep with millimeter fraction accuracy. Applying the method adds value to asset management processes such as as-built drawings and existing geometric structure analysis.

In large-scale work, such as pipeline networks that reach tens and hundreds of kilometers, TLS becomes inefficient in cost and length of work time. Rapid mapping through aerial technologies such as Airborne Laser

Scanning (ALS) and Unmanned Aerial Vehicle (UAV) LiDAR are options. However, the point cloud density of TLS remains 11 times greater than the density of UAV LiDAR and 323 times greater than the density of ALS (K. Calders et al., 2020). The option to find alternative pipeline mapping technology for accurate but also economical mapping needs to be considered.

The use of UAV LiDAR for high-accuracy mapping surveys has been proven across a wide range of applications. From large-scale topographic mapping to landfill analysis for geohazard monitoring, flood management design, and tourism area development plans, UAV LiDAR has demonstrated its versatility. In engineering applications, it has been widely applied, including modeling a 500 kV transmission line network in China (W. Zhang et al., 2017) and France (GIM, 2019), and monitoring bridge deformation to identify potential surface defects (N. Bolourian and A. Hammad, 2020). This versatility makes UAV LiDAR a reliable choice for a variety of mapping and monitoring needs.

The precision of UAV LiDAR point clouds in creating realistic 3-D models is determined by several factors, including flight plan parameters and the accuracy of the laser range measurement. The amount of density is correlated to the detail of the object shape, but does not correlate to the level of accuracy. This means that small or large densities will not increase measurement accuracy, but will enhance the precision of the modeling results. The accuracy of UAV LiDAR measurement results is determined by factors such as GNSS, IMU, and the accuracy of the laser range measurement. Range is the biggest factor influencing the accuracy of the UAV LiDAR point cloud.

The distance the infrared laser travels when fired, hits an object, and then propagates back to the sensor is influenced by environmental factors when the survey is conducted. These factors, such as the object's openness to vegetation cover, weather humidity, and object colour, determine the strength of the infrared laser's reflection to the sensor, ensuring the precision and accuracy of the measurements.

This research analyzed the capabilities of UAV LiDAR for mapping pipelines and support in a three km-long pipeline area. The UAV LiDAR point cloud, with its rapid data acquisition, is used for pipeline and support location detection. In addition, detecting pipeline conditions such as colour, humidity, and vegetation cover uses point cloud density. Next, the point cloud data is used for 3-D pipeline model and supports accuracy in centimeter fractions.

Data and Method

1. Data

The pipeline network of the research stretches 3 km, starting from PAD 29 towards PAD 7, continuing to IJK, and finally towards PAD 31, located at Dieng, Central Java (Figure 1). There are several types of pipeline sizes in the pipeline route. The main pipeline network that distributes hot steam has a diameter of approximately 1 m. The smaller pipes on the left and right of the main pipe with a diameter of roughly 20 cm are used for operational work rather than hot steam distribution. The main pipeline is shiny metallic, matte green, and tends to be white, while the small diameter pipe is black.

Pipelines and pipes support as a single pipeline network. The support's size, shape, and height vary depending on the terrain's topography, the number of pipes supported, and the purpose of the support. Some pipelines are attached to the ground or above the ground, and some are curved vertically at road intersections (Figure 2).

2. GNSS measurement for control point

This study shows that GCPs and ICPs are evenly distributed throughout the area of interest, especially in the corners of the area, and are a depiction of terrain variations (Figure 3). This study installed 14 control points: GCP, ICP, and TLS to test the accuracy of the cloud data. In addition to check points, there is one control point

used as a base station during UAV LiDAR acquisition. Check points are installed with premarks made of tarpaulin with shiny colours.

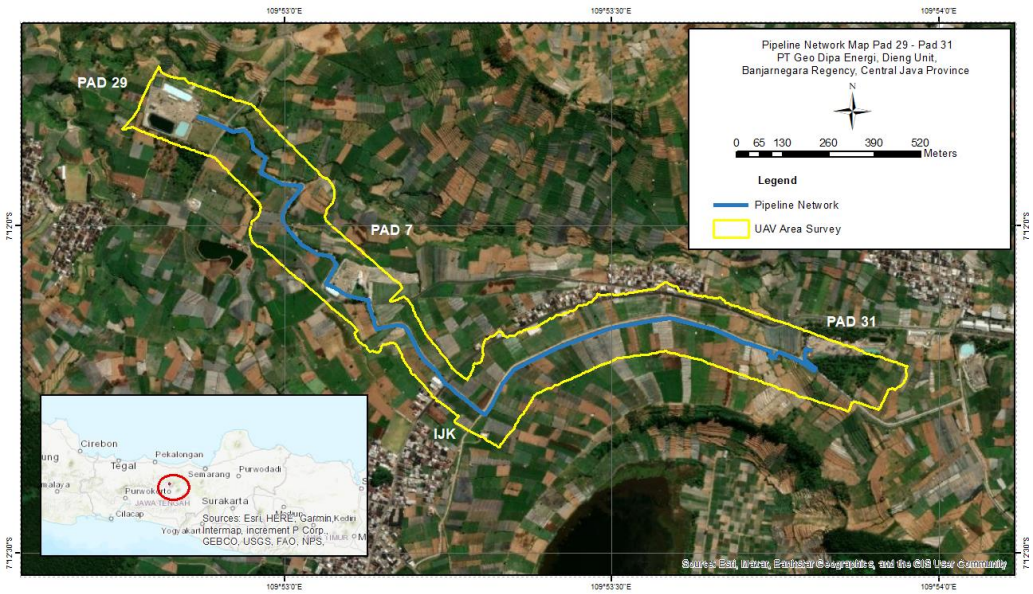

Figure 1. Pipeline network and UAV LiDAR survey area overlay with world imagery.

Figure 2. Pipeline network: (a) an open area with a shiny metallic colour; (b) a curved vertical pipeline at a road intersection with matte colour; (c) the steam pipe is above ground supported by its support and the water pipe is below the steam pipe; (d) segments of the steam pipe and water pipe are covered by vegetation so that they cannot be seen from above.

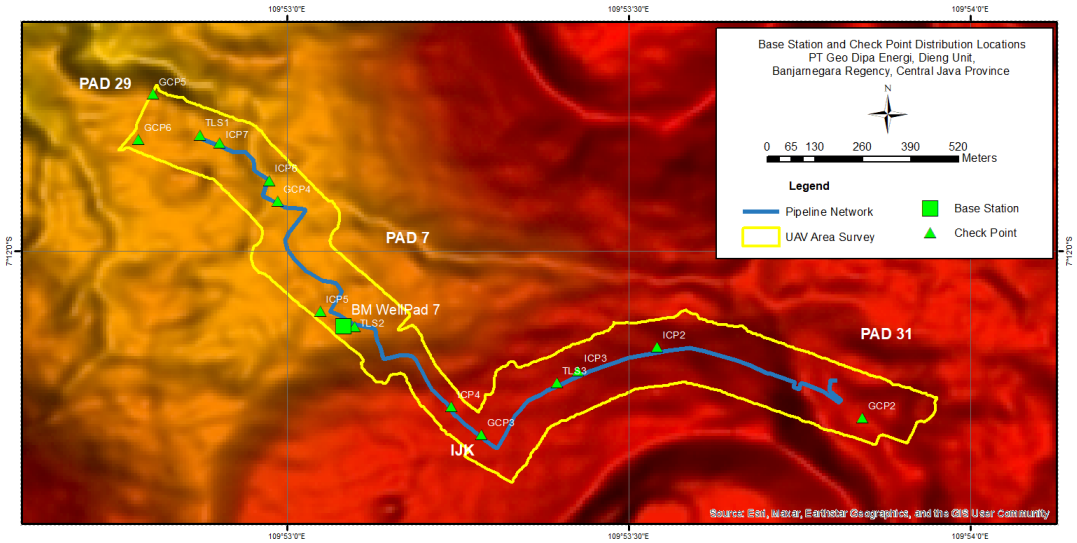

Figure 3. Distribution of check points at the study location and their placement, taking into account the topographic terrain form.

All control points are measured using GNSS which is referenced to the national coordinate system applicable in Indonesia: the Indonesian Geospatial Reference System (SRGI) from the Geospatial Information Agency. The vertical reference used is INAGEOID2020. GNSS observations at the base station refer to five CORS stations around the location, namely CORS CBJN in Banjarnegara, CORS SMG and CORS CSEM in Semarang, CORS CPKL in Pekalongan, and CORS CMGL in Magelang with an observation period of five hours. Furthermore, the base station point is a reference for measuring GCP and ICP networks with an observation period of 30 minutes. The GNSS processing results in the average error in the X coordinate, 4.7 mm, in the Y coordinate, 3.9 mm, and in the Z coordinate, 17.6 mm.

3. UAV LiDAR survey

UAV LiDAR survey was conducted along the research pipeline network with a 100 m left and 100 m right corridor. The total survey area was 44.68 ha. The equipment used was the Alpha Unit 20 (AU20) CHC flown using CHC BB4. The LiDAR system and aerial camera are integrated into one unit. The POS-AV system uses NovAtel SPAN (CPT7/HG4930) with GNSS recording every 1 second and INS data recording every 1/600 second. The laser can fire 2,000,000 pulses/second with 16 target echoes. The aerial camera pixel size reaches 45 MP.

LiDAR was flown at an altitude of 70 m AGL divided into three flight missions. Data acquisition was carried out on April 2, 2024. Because the geothermal power plant was still operational when the data collection was carried out, thick water vapor came out of the chimney of the PAD area. The air was lightly foggy at the time of data acquisition.

The total time required for the acquisition of an area of 44.68 ha was 77.9 minutes, a testament to the thoroughness of our data acquisition process. We acquired a total of 1639 frames, ensuring comprehensive coverage of the survey area. The technical specifications for the implementation of UAV LiDAR and aerial photo acquisition can be seen in Table 1.

Table 1. UAV LiDAR and aerial photo flight parameters used in the research

Parameter	Setting
Flying height	70 m AGL
Flying speed	7 to 8 m/s
Width coverage	150 m
Sidelap LiDAR	70%
Overlap/sidelap photo	80%/70%
Acquisition mode	Discrete return 16 echoes
Raw photo GSD	5 cm
Battery capacity per mission	25 to 30 minutes

4. UAV LiDAR data processing

Flight trajectories were determined using dedicated software from CHC manufacturer CoPre. Trajectories are a combination of XYZ coordinates of the GNSS sensor and orientation to the XYZ axis of the IMU sensor. The trajectory is a reference for the position and orientation of the LiDAR and aerial photo sensors. Average trajectory adjustments were 10 mm for positions and 0.01 degrees for angles. The recorder receives the pulse feedback, translated into a point cloud with 3-D XYZ coordinates. Furthermore, with the same software, misalignment correction was performed by finding the difference dX, dY, dZ, dθ (mirror) between flight paths

and correcting them using the cloud-to-cloud method iteratively. The average misalignment error was 23 mm. The point cloud of the measurement classes are ground, support and pipelines, also non-ground.

Classification uses TerraSolid v.019 software, operated in Microstation v8 software, meticulously and thoroughly. The process is semi-automatic, with the first step being automatic classification using the distance and angle algorithm between point clouds. The classification sequence starts from low point classification, ground classification, non-ground classification, and pipeline classification. This automatic classification is performed iteratively, ensuring that every detail is noticed. Furthermore, the point cloud is subjected to quality control of the classification results. If a point cloud is in the wrong class, it will be reclassified manually. To assist point cloud classification, an orthophoto with GSD 7 cm is used as a reference for object identification. Figure 4 shows the visualization of point cloud intensity in the study area, an enlarged pipeline segment using colouring photo point cloud, and shiny metallic colour in an open area.

5. Pipeline 3-D modelling

Figure 4. Visualisation of: (a) point cloud intensity in study area and; (b) an enlarged pipeline segment using colouring photo point cloud; (c) shiny metallic colour in an open area.

The pipeline is meticulously modelled in two formats namely mesh and solid models. The mesh model, a testament to the precision of the point cloud obtained, reconstructs the pipeline according to the input data provided. The level of detail in the mesh model is directly proportional to the proximity of the point clouds. A close distance between point clouds results in a highly detailed mesh model, while a sparse distance yields a coarser representation.

The mesh model pipeline was meticulously crafted using the powerful Cloud Compare software v.2.12.4. The algorithm used is Poisson reconstruction (Cloud Compare, 2017) with octree depth level 12. The minimum number of sample points that should fall within an octree node as the octree construction is 1.5 samples. Interpolation weight using b-spline degree 2.

While the 3-D solid model is not a natural form of point cloud density reconstruction, it is an ideal surface model. The position and distribution of the point cloud will be a reference for detecting and drawing solid models. However, the shape and detail of the 3-D solid will be taken from the model with the existing model in the library. 3-D solid model uses AutoDesk Revit software. Figure 5 shows the results of the 3-D mesh

pipeline in an open area. While Figure 6 shows the process of modelling a pipeline with a vertical curved shape, starting from point cloud to solid model generation.

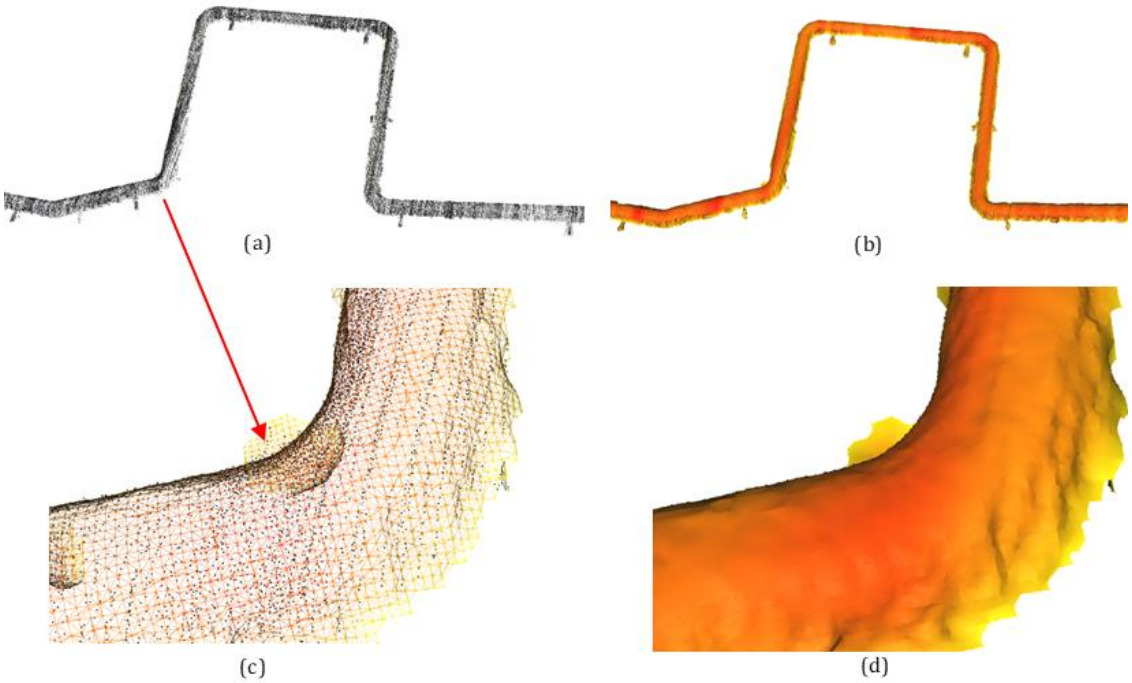

Figure 5. Visualisation of: (a) point cloud pipeline and support; (b) 3-D mesh model (a); (c) triangulation network forming 3-D mesh; (d) 3-D mesh model.

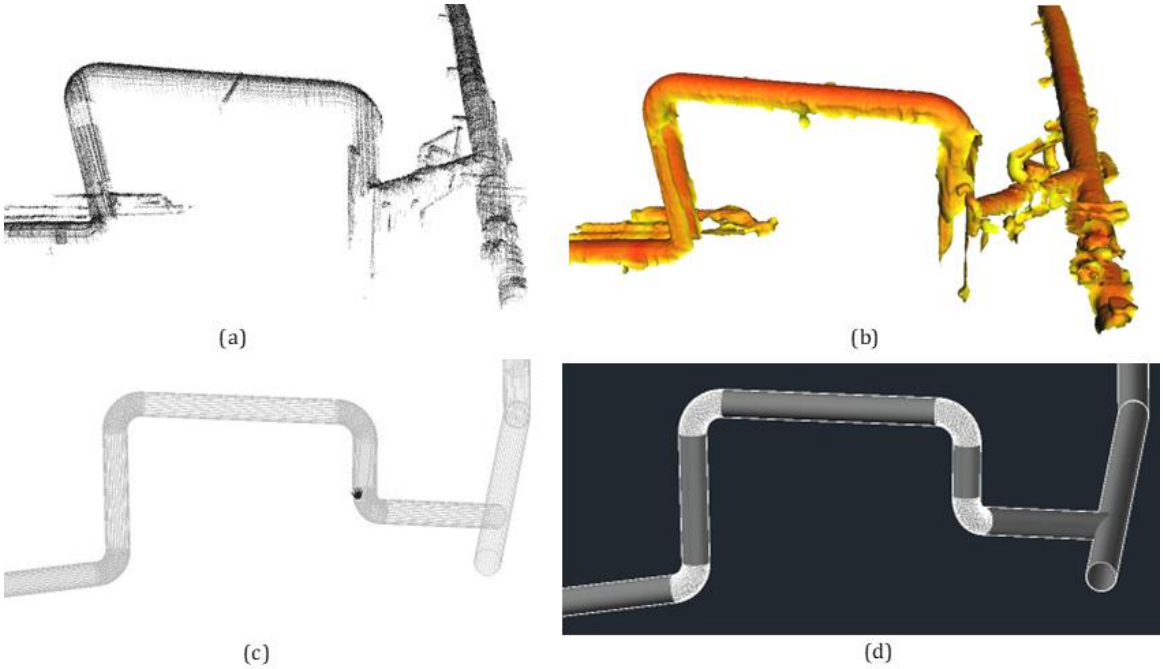

Figure 6. Visualisation of: (a) point cloud pipeline and support; (b) 3-D mesh model (a); (c) triangulation network forming 3-D mesh; (d) 3-D mesh model.

Result and Analysis

1. Detect the position of pipelines network and support

UAV LiDAR point cloud can quickly detect the presence of the main pipeline and its support. Small diameter pipelines can also be detected, although only on the top side and not forming a complete round pipe. What is important to note is that the point cloud can get a pipeline size of less than 20 cm with a distance between pipes of only 5 cm (Figure 7).

Furthermore, in the pipe segments stacked above and below, where the upper pipe will cover the appearance of the pipe below, it can be detected in the point cloud. This kind of pipe stack is not visible in the orthophoto. Figure 8 shows seven pipes visible in the orthophoto, but from the point cloud, nine pipes are detected. The field data shows that the total number of pipes is nine, the same as the point cloud results.

In segments covered by dense vegetation and where no objects are visible underneath, the point cloud is still able to detect the main pipeline and its support. Likewise, small pipes can still be detected. However, if the vegetation cover is mixed with bushes, the pipeline point cloud becomes mixed with the bush point cloud, which is challenging to detect. The pipeline position identification guide is seen from the empty round shape in the middle, like a solid cylinder. Figure 9 shows the pipeline position can still be recognized in small pipes stacked under vegetation, although it does not form a cylindrical pattern.

The position of the main pipeline and its support are then presented in a longitudinal profile map. The information presented includes ground elevation, pipeline position, and elevation from above ground, support position, and ID number. Ground elevation information in contours and digital elevation models (DEM) is obtained from processing ground-class LiDAR data. The digital surface model (DSM) is created using all point cloud classes except low points.

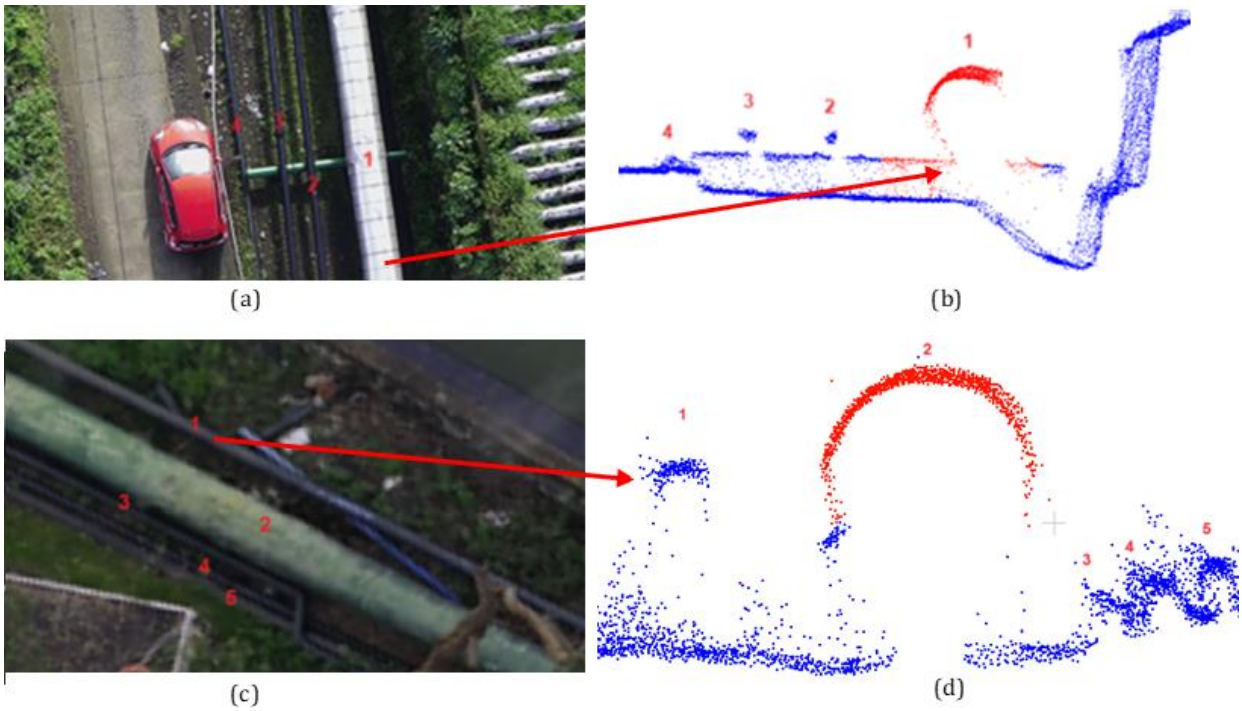

Figure 7. Pipeline position and support in an open area: (a) as many as four pipes are visible in the orthophoto; (b) as many as four pipes are visible in point cloud; (c) the distance between pipelines number 3, 4, and 5 is approximately 5 cm in the orthophoto; (d) all pipes are visible in the point cloud even though the distance between the pipes is only 5 cm.

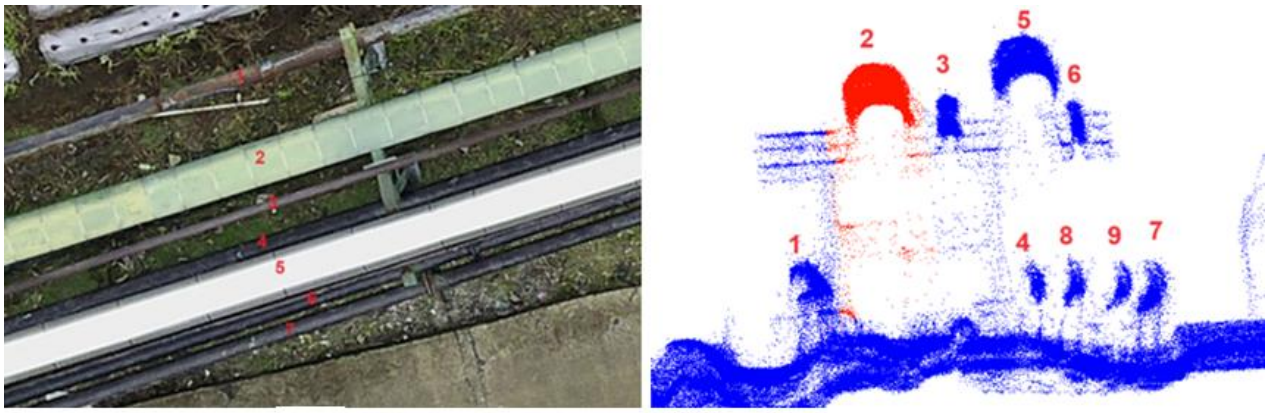

(a) (b)

Figure 8. The pipe segments that are stacked above and below: (a) on orthophoto shows seven pipes; (b) the point cloud profile shows nine pipes and this number is the same as the number of pipes in the field.

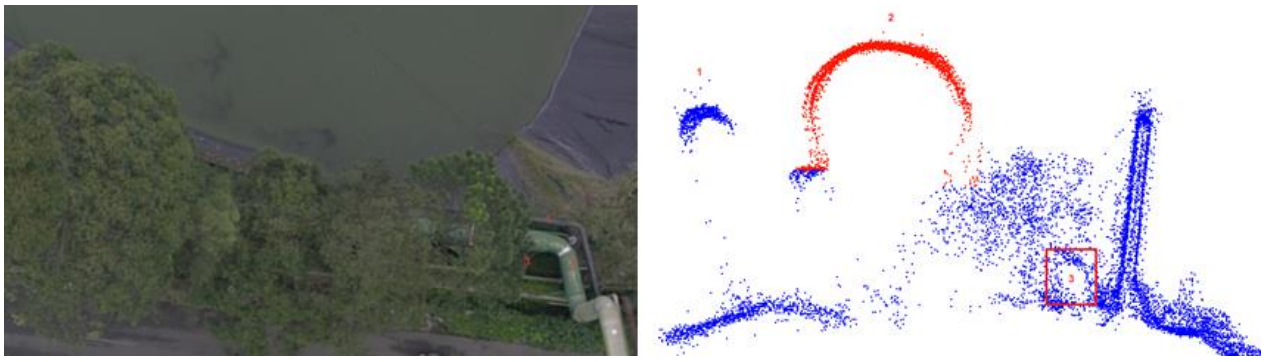

(a) (b)

Figure 9. The pipe segments under dense vegetation: (a) top view on orthophoto shows three pipes; (b) the point cloud profile shows three pipes including the small pipe around bushes.

Figure 10 shows the point cloud of the main pipeline and its support. The height and width of the support can be calculated from this point cloud. While Figure 11 shows the longitudinal profile map, DSM, and DEM of the study area.

2. Point cloud density

Point cloud density is one of the determining factors in the detailed results of 3-D model. Although density does not affect the level of accuracy of the data results (J. J. Sofonia et al., 2019), it increases the detail of the object reconstruction results. The more detailed, the more precise the reconstruction results.
Point cloud density varies across different environments, each presenting unique challenges and opportunities for 3-D model. In an open area (samples taken on concrete roads and asphalt roads), the average density is 1359 points/m^2 with a distance between points of 2.4 cm. If dissected again, the density on bright concrete roads (high intensity) is 1466 points/m^2, while on dark asphalt roads (low intensity) it is 1011 points/m^2. In dense vegetation with bushes underneath, the average density reaches 9371 points/m^2, and the distance between points is 8 mm. In medium vegetation, which is only tall plants without bushes, the average density is 4644 points/m^2.

The 1 m diameter metallic coloured pipeline is located on the IJK towards Pad 31 segment. In this segment, the pipeline is held by supports with relatively flat topography. This segment's average point cloud density is around 2027 points/m^2. Meanwhile, the 1 m diameter with a dull matte colour, approaching white, is located

on the Pad 7 towards IJK segment. The average point cloud density is 2226 points/m^2. For the 1 m diameter matte coloured pipeline, it is located in front of Pad 7 with a point cloud density of 1491 points/m^2.

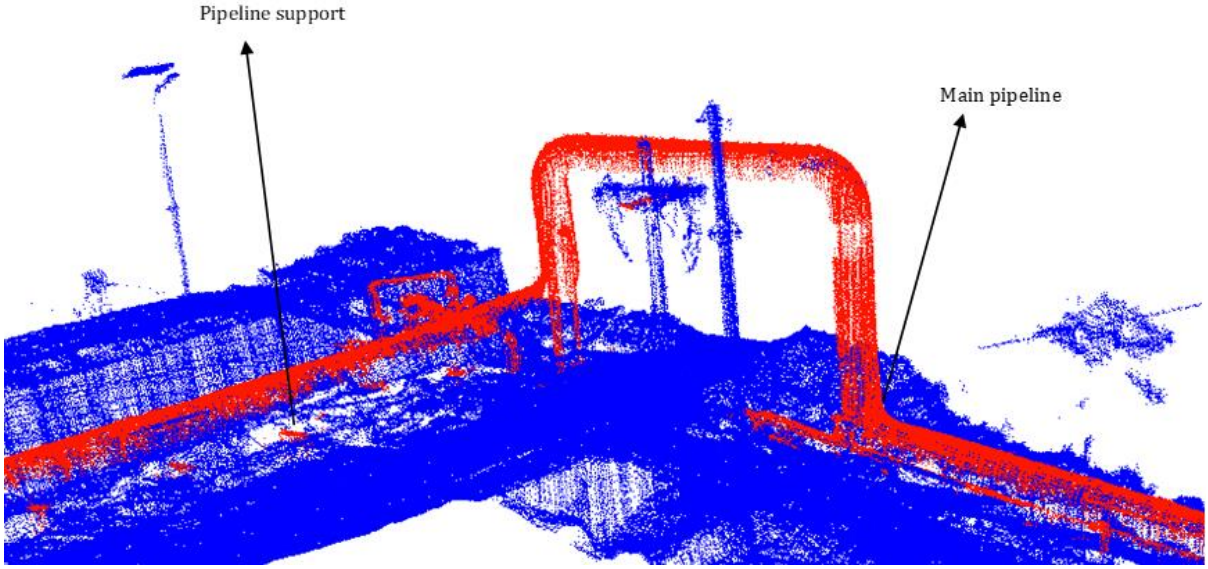

Figure 10. The main piping and its support point cloud in red colour. Support dimensions: its width and height from the ground can be calculated directly.

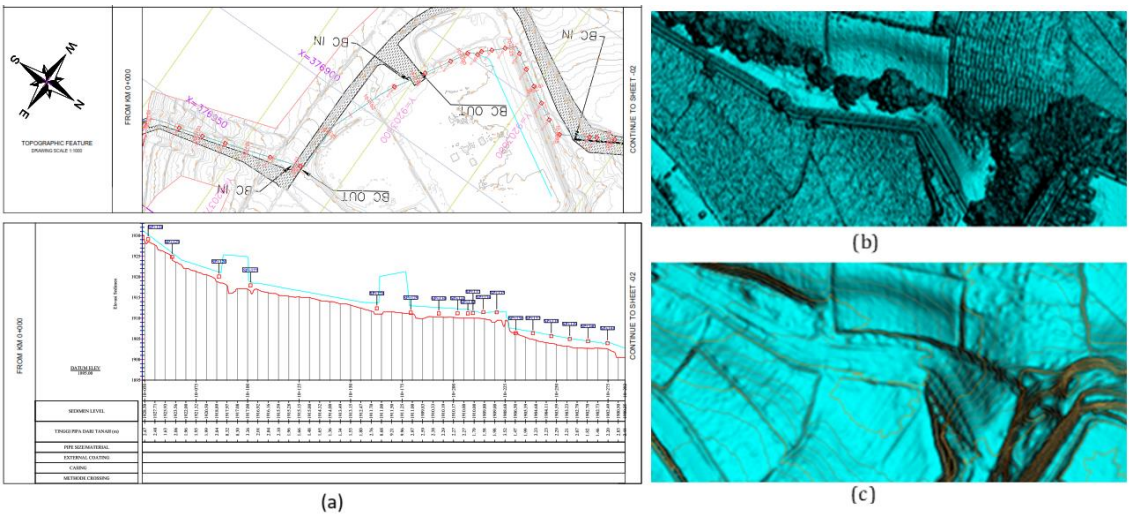

Figure 11. The pipe segments under dense vegetation: (a) top view on orthophoto shows three pipes; (b) the point cloud profile shows three pipes including the small pipe around bushes with DSM. (c) the point cloud profile shows three pipes including the small pipe around bushes with DTM.

The main matte pipeline under dense vegetation, a crucial data point, has an average density of 1273 points/m^2. This average is only 17% less than the average density of the matte pipeline in open areas. The density identification sample recap is calculated with a reference to a 1 m x 1 m polygon and is spread across the main pipeline network with a diameter of 1 m. Details of the samples used are as in Tables 2 and 3.

Table 2. Recap of point cloud density in an open area and under vegetation

Segment	No. Sample	Parameter	Density (per m^2)	Point Spacing (m)
		Open Area		
IJK – Pad 31	Sample 1	Flat topography concrete road, bright intensity	1698	21.25
	Sample 2	Flat topography concrete road, bright intensity	1486	23.01
	Sample 3	Flat topography concrete road, bright intensity	1752	23.89
IJK – Pad 7	Sample 4	Concrete road topography downhill, bright intensity	1886	19.51
	Sample 5	Concrete road topography downhill, bright intensity	1441	21.86
	Sample 6	Flat topography concrete road, bright intensity	1447	19.95
Pad 7 – Pad 29	Sample 7	Concrete road topography downhill, dark intensity	1132	26.83
	Sample 8	Concrete road topography downhill, dark intensity	1048	26.92
	Sample 9	Concrete road topography downhill, bright intensity	1421	23.8
IJK – Pad 7	Sample 10	Concrete road topography downhill, bright intensity	1355	27.17
	Sample 11	Flat asphalt road, dark intensity	925	29.57
	Sample 12	Flat asphalt road, dark intensity	956	27.74
	Sample 13	Flat asphalt road, dark intensity	1152	26.31
	Sample 14	Flat asphalt road, bright intensity	1337	22.52
		Vegetation		
	Sample 15	Dense vegetation and shrub	9371	0.00815
	Sample 16	Dense vegetation, tall tree	6899	0.00971
	Sample 17	Medium vegetation	5774	0.01096
	Sample 18	Medium vegetation	4581	0.01069
	Sample 19	Medium vegetation	3577	0.0118

Table 3. Recap of point cloud density on 1 m diameter pipeline

Segment	No Sample	Parameter	Density (per m^2)	Point Spacing (mm)
		Open Area		
IJK – Pad 31	Sample 1	Metallic	1926	18.23
	Sample 2	Metallic	2102	18.17

	Sample 3	Metallic	2058	17.67
IJK – Pad 7	Sample 4	Matte tends to white	2168	14.87
	Sample 5	Matte tends to white	1740	19.46
	Sample 6	Matte tends to white	2771	12.6
	Sample 7	Matte	1256	25.26
	Sample 8	Matte	1727	16.21
		Vegetation		
IJK – Pad 7	Sample 9	Under vegetation	967	021.65
	Sample 10	Under vegetation	1294	14.52
	Sample 11	Under vegetation	1253	17.95

3. Result of 3-D mesh model and 3-D mesh solid pipeline

The point cloud from the UAV LiDAR acquisition only provides information from the top and a little from the left and right sides of the pipeline, while the bottom is empty. Therefore, the 3-D mesh model that is formed is only the top part, unable to create a full cylinder. For the main pipeline on the Pad 7-IJK-Pad 31 segment, the 3-D mesh of the pipeline can be formed as a network in its entirety, both in open areas and in vegetation (Figure 12).

The results of 3-D mesh model of pipes with a diameter of less than 20 cm depend on the density quality obtained. In small pipes, the density obtained tends to be rare and only on the upper side. Therefore, the point cloud is insufficient to create a 3-D mesh model. Figure 13 shows that the small pipe modelling seals are broken and cannot form a longitudinal pipeline pattern.

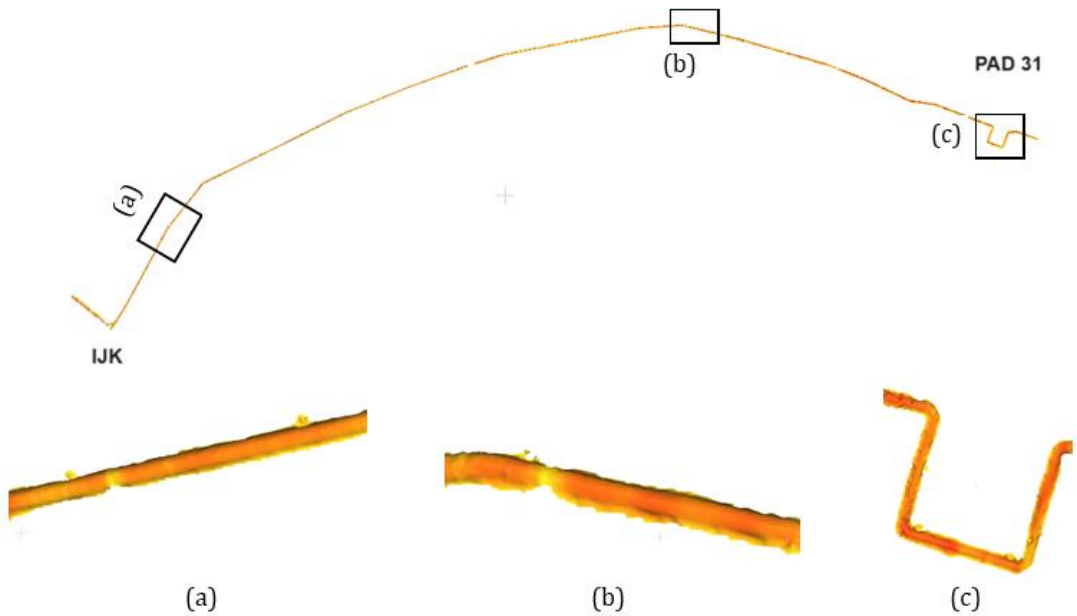

Figure 12. 3-D mesh model of the main pipeline on the IJK towards Pad 31 segment with an open area and flat topography.

In the case of pipes with a diameter of less than 20 cm under dense vegetation, the successful classification of the point cloud is crucial in forming a 3-D mesh model. However, if the point cloud on a small pipe can be obtained from many sides, not just the top side, then a 3-D mesh model can be formed. Eventough the location of the small pipe was under vegetation. Figure 14 shows that a 3-D mesh model of a small pipe under vegetation can be formed because the pipeline point cloud was successfully obtained.

In this study, the solid modeled pipeline is the main pipeline. The small pipelines are not included in the modelling. Since the point cloud of the main pipeline can be obtained well, its 3-D solid model can also be formed for the entire research area (Figure 15).

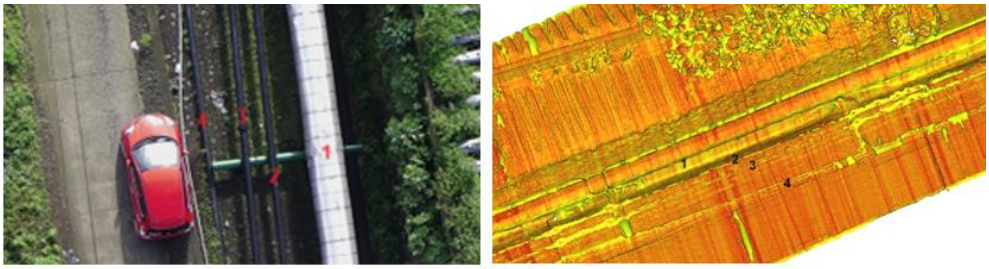

(a) (b)

Figure 13. Main pipeline and small pipes in an open area: (a) on orthophoto; (b) 3-D mesh model of the main pipeline is well formed into a pipeline network, but the three small pipes next to it cannot be formed as a network.

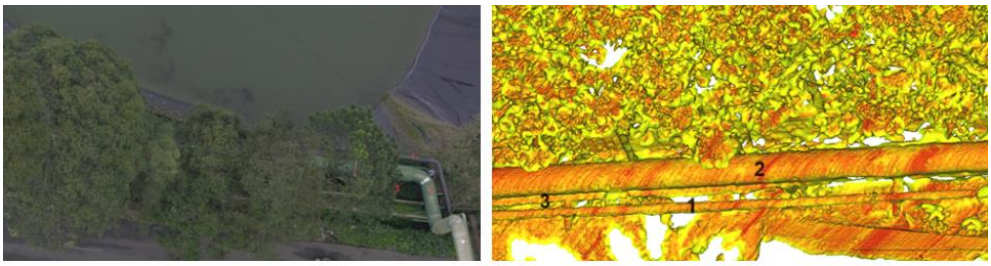

(a) (b)

Figure 14. Main pipeline and small pipes under vegetation: (a) on orthophoto; (b) 3-D mesh model of the main pipeline is well formed into a pipeline network, and the three small pipes next to it still can be formed as a network.

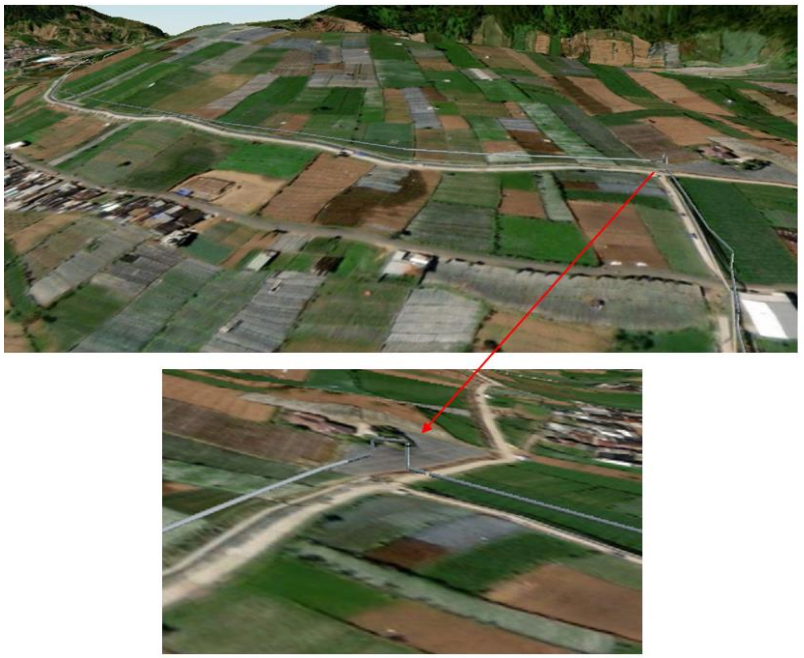

Figure 15. 3-D solid model of the entire research pipeline network overlay in Google Earth.

4. Point cloud density conditions influenced by water vapor

During data acquisition, the geothermal power plant in the study area was actively operating and there was residual hot water vapor from combustion released at Pad 29 and Pad 7. The characteristics of infrared waves used in UAV LiDAR are easily absorbed by water elements. The hypothesis is that there will be no point cloud on objects covered by water vapor. However, the analysis at Pad 29 revealed an unexpected finding: the result was able to obtain a detailed point cloud of objects under the water vapor, including piping, combustion chimneys, and ground. The finding challenges our understanding and opens up new possibilities for data acquisition in similar conditions. Although on the top side of the chimney, exactly where the water vapor comes out, the laser beam cannot penetrate it, and there is no point cloud there (Figure 16.b. red polygon). Empty point clouds occur in water pools and puddles of rainwater (Figure 16.b. yellow polygon).

Different things happened on Pad 7 (Figure 17). The hot water vapor from the chimney was thicker and had a more comprehensive coverage range. LiDAR point cloud data and aerial photos taken from two flight plan directions still could not provide information on objects under the water vapor. The point cloud data was empty on the chimney side, and all objects were under the water vapor. This data gap is similar to when an infrared laser hits a pool of water or puddle.

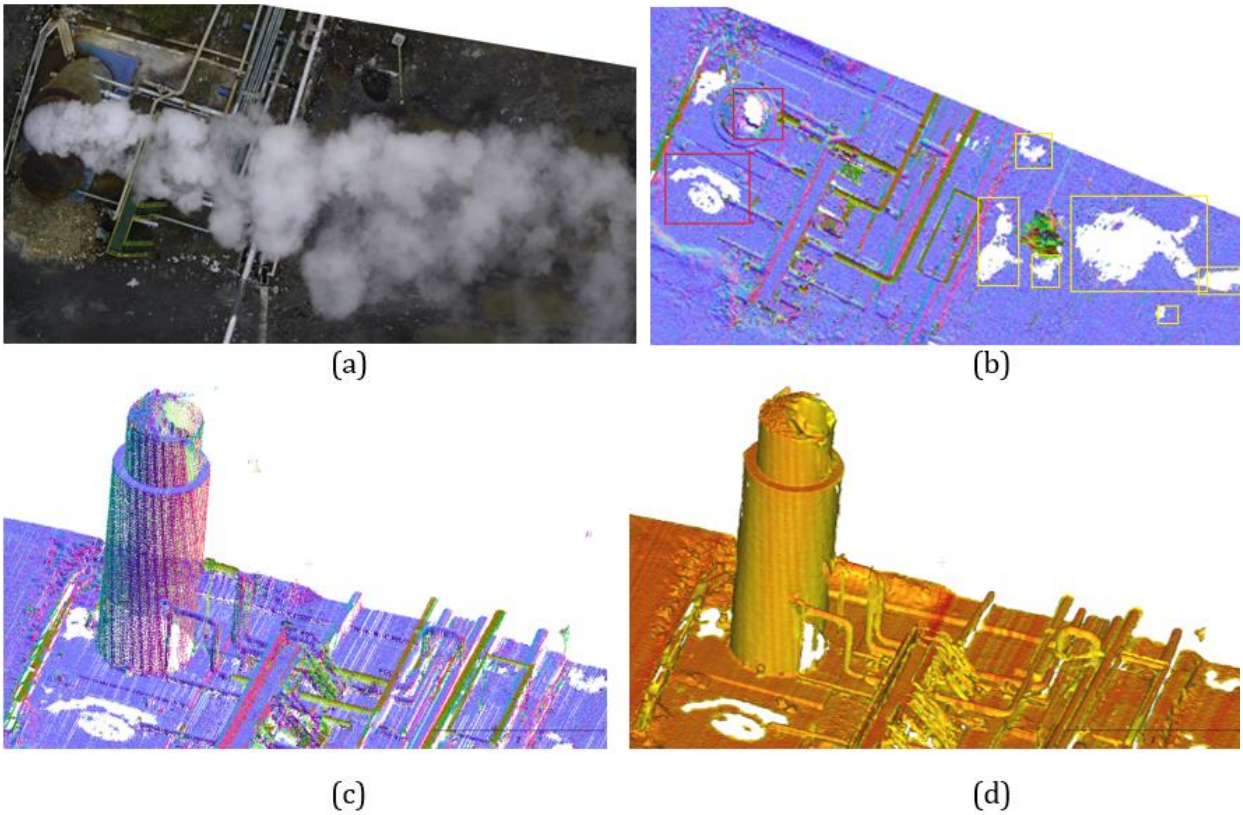

Figure 16. Geothermal combustion operations in Pad 29: (a) water vapor comes out of the chimney covering the objects below it, (b) point cloud top view, red polygons show empty data due to the influence of water vapor, while yellow polygons show empty data due to rainwater puddles, (c) side view of the chimney, piping, and objects below the water vapor still get point cloud data, (d) 3-D mesh model of the chimney, piping, and other objects is still being formed.

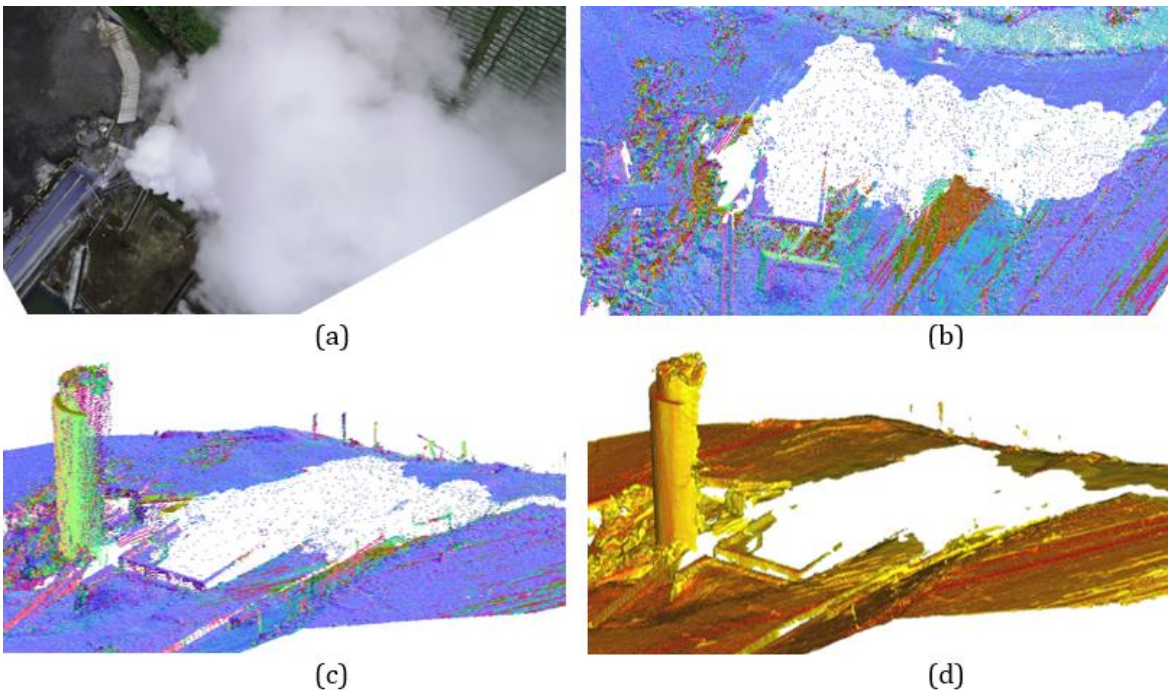

Figure 17. Geothermal combustion operations in Pad 7: (a) the water vapor that comes out is thicker with a wider range than that on Pad 29, (b) the top view of the point cloud shows empty data on the object below the water vapor, (c) the side view of the object below the water vapor shows no point cloud data, (d) the 3-D mesh model of the chimney is only half formed.

5. UAV LiDAR mapping accuracy

The vertical accuracy of the UAV LiDAR mapping results is calculated by comparing the premark Z-coordinates with the point cloud Z-coordinates. The statistical test was conducted to determine the root mean square error value by comparing elevation field data with LiDAR data. From 14 checkpoints, the RMSE value was obtained as 0.070 m. The RMSE value was then used to calculate the linear error at a confidence level of 90%. The linear error accuracy of UAV LiDAR mapping is 0.115 m. This accuracy value has met the standard for a large-scale map of 1:1000 from the Geospatial Information Agency-the formula for calculating RMSE in Equations 1 (BIG, 2018, BSN, 2019).

$$RMSE = \sqrt{\frac{\sum_{i=1}^{N}(X_i - \hat{X}_i)^2}{n}} \quad (1)$$

Where:

$RMSE$: root mean square, measures the average magnitude of the error
X_i : the actual value of its observation
$\hat{X}_i$: the predicted value for the its observation
n : the number of observations

A summary of the elevation difference between the point cloud and check points can be seen in Table 4.

Table 4. UAV LiDAR point cloud elevation accuracy test results with check points

Point	Easting (m)	Northing (m)	Known Z (m)	Laser Z (m)	DZ (m)
GCP2	378259.920	9203544.725	2103.828	2103.890	+0.062
GCP3	377232.972	9203496.472	2027.635	2027.710	+0.075
GCP4	376681.945	9204124.690	1884.787	1884.820	+0.033

GCP5	376345.449	9204413.325	1895.320	1895.250	-0.070
GCP6	376306.293	9204290.093	1890.649	1890.710	+0.061
ICP2	377706.672	9203734.230	2056.191	2056.220	+0.029
ICP3	377494.123	9203670.479	2048.173	2048.230	+0.057
ICP4	377152.717	9203572.562	2012.135	2012.220	+0.085
ICP5	376798.216	9203828.630	1905.519	1905.460	-0.059
ICP6	376660.134	9204180.889	1883.641	1883.630	-0.011
ICP7	376526.231	9204281.377	1892.608	1892.610	+0.002
TLS1	376472.611	9204302.753	1894.614	1894.620	+0.006
TLS2	376890.940	9203788.494	1916.125	1915.940	-0.185
TLS3	377436.743	9203637.461	2045.489	2045.510	+0.021

6. Paired sample t-test

The paired sample t-test is generally used to compare the values of two measurements taken from the same individual, object, or related unit (P. S., Mann, 2014). In this study, this statistical test is used to test whether the elevation of the two methods is significantly different. In general, it is important to know whether the elevation from the premark coordinates with the point cloud coordinates (Table 4). Specifically in this study, this statistical test aims to check whether the elevation difference between the point cloud with check points differ significantly in coordinates and whether the resulting precision is appropriate.

The statistical test was conducted using a 95% confidence level with $df = n\text{-}1 = 13$ degrees of freedom so that the student t-table value = 2.16 was obtained. If the value of $t_{compute}$ > t-table indicates that the elevation difference between the point cloud with check points significantly differs, the formula for the paired sample significance test is presented in Equations 2 and 3 (W. Su, 2024).

$$t_{compute} = \left| \frac{\overline{D_Z}}{S_{\overline{D_Z}}} \right| \quad (2)$$

$$t_{compute} \leq t_{\left(\frac{\alpha}{2}, df\right)} \quad (3)$$

Where:

$\overline{D_Z}$: the average of elevation difference between the point cloud, GCP, and ICP
$S_{\overline{D_Z}}$: the standard deviation of elevation difference between the point cloud, GCP, and ICP
$t_{compute}$: the calculated t value, the statistical value from the student t-table is represented by the notation in the right-hand side of Equation 3

$$t_{compute} = \left| \frac{0.054}{0.046} \right| = 1.16$$

The paired sample t-test results indicate that the elevation difference between the point cloud with check points does not differ significantly. Specifically, the $t_{compute}$ value for the elevation component of the 14 points is 1.16, less than the t-value threshold of 2.16. However, the elevation components have no significant difference, as the values are smaller than the specified threshold.

Conclusions

The results of the study show that the main pipeline point cloud can be obtained from UAV LiDAR surveys and aerial photos, both in open areas and in areas under dense vegetation. The average density of the main pipeline point cloud with the same colour under vegetation is only 17% less than that of the pipeline in open areas. Of the total point clouds in all classes, the total pipeline point cloud reaches 21%. It makes the position and shape of the main pipeline under vegetation similar to that of the pipeline in open areas.

Pipes with a diameter of less than 20 cm in open areas have successfully obtained point clouds, although only the upper side. However, these results can already calculate their position and height above the ground. However, small pipelines cannot be modelled adequately in 3-D mesh and have yet to be able to form a complete pipeline path.
Objects under hot water vapor with strong density cannot be penetrated by LiDAR infrared laser light because the steam absorbs them. This results in the point cloud below being empty. However, if the water vapor density level is not too high, the LiDAR point cloud is still able to provide detailed information on the objects below.

The total time required for UAV LiDAR data acquisition in the research area was 77.9 minutes, divided into three survey missions. The fieldwork, starting from the preparation stage; health, safety, and environment induction; reconnaissance survey; GNSS control point survey; LiDAR data acquisition; aerial photography; and pre-processing in the field, took two working days. The time required for point cloud classification was three days. The creation of a longitudinal profile map of the pipeline took three days. The total work time was eight days from preparation to the longitudinal profile map presentation. This total time does not include the creation of a 3-D data model. Mapping using UAV LiDAR and aerial photography can answer the need for rapid data acquisition to map the pipeline network and its supports accurately. Information on pipeline position, position relative to the ground, support position, and support height on the main pipeline network can be obtained for the entire network in the research area. The method applies not only to segments in open areas but also to segments in areas covered by vegetation where the orthophoto cannot display the presence of the pipeline, but the LiDAR point cloud can identify it. In this research, the 3-D mesh and 3-D model in the main pipelines can also be formed well.

The paired sample t-test results indicate that the elevation difference between the point cloud and check points does not differ significantly. Specifically, the $t_{compute}$ value at the 95% confidence level for the elevation component of the 14 points is 1.16, less than the t-value threshold of 2.16. Meanwhile, the RMSE elevation value is 0.070 m and the linear error accuracy at the 90% confidence level is 0.0115 m.

Acknowledgment

We would like to thank PT Geo Dipa Energi, Dieng Unit, PT Terra Data Persada, and PT Jelajah Semesta Teknologi for performing UAV LiDAR and aerial photo data acquisition in the study area.

References

BIG, 2018, Regulation of the Head of the Geospatial Information Agency, No. 6:2018.

BSN, 2019, Base Map Accuracy, National Standardization Agency SNI 8202:2019.

Cloud Compare Document, 2017, Extract Sections, [https://www.cloudcompare.org/doc/wiki/index.php/Extract_Sections# Generating_cloud_slices_and_profiles].

GIM, 2019, International Magazine, French Experiences with UAV LiDAR for Power Line Inspection, [https://www.gim-international.com/content/news/french-experiences-with-uav-lidar-for-power-line-inspection].

J. J. Sofonia, S. Phinn, C. Roelfsema, F. Kendoul, and Y. Rist, 2019, Modelling the Effects of Fundamental UAV Flight Parameters on LiDAR Point Clouds to Facilitate Objectives-based Planning, ISPRS Journal of Photogrammetry and Remote Sensing, Elsevier. Vol. 149, 105-118.

K. Caldersa, J. Adams, J. Armston, H. Bartholomeus, S. Bauwens, L. P. Bentley, J. Chave, F. M.Danson, M. Demola, M. Disney, R. Gaulton, S. M. K. Moorthy, S. R. Levick, N. Saarinenn, C. Schaaf, A. Stovall, L. Terryn, P. Wilkes, and H. Verbeeck, 2020, Laser Scanning in Forest Ecology: Expanding the Horizon, Remote Sensing of Environment, Elsevier, Vol. 251, 11210.

N. Bolourian and A. Hammad, 2020, LiDAR-Equipped UAV Path Planning Considering Potential, Automation in Construction, Elsevier, Vol. 117, 103250.

P. S. Mann, 2014, Introductory Statistics,Seventh Edition. New Jersey. Wiley.

W. Su, 2024, Introduction to Applied Statistics: Open Textbook Series in Statistics.

W. Zhang, X. Wu, G. Zhang, L. Ke, L. Chen, X. Chen, H. Yang, X. Qiao, and Y. Zhou, 2017, The Application Research of UAV-based LiDAR System for Power Line Inspection, 2nd International Conference on Computer Engineering, Information Science & Application Technology, Vol. 74.